Non-destructive monitoring of delamination healing of a CFRP composite with a thermoplastic ionomer interlayer

Post, W.; Kersemans, M.; Solodov, I.; Van Den Abeele, K.; García, S. J.; van der Zwaag, S.

DOI
10.1016/j.compositesa.2017.06.018

Publication date
2017

Document Version
Accepted author manuscript

Published in
Composites Part A: Applied Science and Manufacturing

Postprint of Composites Part A: Applied Science and Manufacturing
Volume 101, October 2017, Pages 243-253
Link to formal publication (Elsevier): https://doi.org/10.1016/j.compositesa.2017.06.018

Non-destructive monitoring of delamination healing of a CFRP composite with a thermoplastic ionomer interlayer

W. Post[1], M. Kersemans[2], I. Solodov[3], K. Van Den Abeele[4], S. J. García[1], S. van der Zwaag[1]

[1]Novel Aerospace Materials Group, Faculty of Aerospace Engineering, Technical University of Delft, Kluyverweg 1, 2629 HS, Delft, The Netherlands

[2] Department of Materials, Textiles and Chemical engineering – MaTCh, Ghent University, Technologiepark-Zwijnaarde 903, 9052 Zwijnaarde, Belgium

[3]Institut für Kunststofftechnik, Universität Stuttgart
Pfaffenwaldring 32, 70569 Stuttgart, Deutschland

[4]Wave propagation and Signal Processing, Department of Physics, KU Leuven campus KULAK, Etienne-Sabbelaan 53, 8500 Kortrijk, Belgium

Abstract

A comparative study is performed on the monitoring of delamination healing in CFRP-ionomer sandwich composites by non-destructive techniques and destructive compression testing. Artificial delaminations of various areal dimensions and nature were introduced during production of the composites. The extent of the delamination and the healing thereof was monitored in both air and water-coupled ultrasonic C-scan experiments as well as by the frequency shift of the local defect resonance (LDR). It is shown that the LDR approach can be used to detect the early stage healing of the delaminations while ultrasonic C-scanning techniques are very effective to determine the extent of healing in the final stages of the repair process. A quasi-linear relation was observed between the delaminated area measured with ultrasonic C-scan and the compressive failure strength in destructive testing. This correlation shows the beneficial effect on the compression strength of the delaminated area reduction by on-demand healing.

Keywords: Self-Healing; Polymer-matrix composites; Non-destructive testing;

1. Introduction

For more than two decades Fibre Reinforced Polymer Composites (FRPCs) have emerged in many engineering constructions, and now have become an indispensable option in modern design strategies for advanced load bearing light weight products because of their low relative density, high strength and high stiffness [1,2]. However, a major disadvantage of FRCPs is that they are sensitive to impact, leading to barely visible impact damage, matrix cracking and delaminations which can ultimately result in catastrophic failure of the component without much prior notification [3,4]. In order to prevent such a failure mode, FRPCs are often over-dimensioned or subjected to periodic non-destructive testing (NDT). Alternatively, to raise the impact resistance and interlaminar fracture toughness of FRPC's, thermoplastic interlayers in between the composite plies have been proposed [5,6]. The interlayers lower the overall mechanical properties but prevent wide spreading of the impact damage as they 'contain' the damage by delamination at the interlayer-FRPC interface or by internal damage[7]. A further and as-yet barely explored advantage of such thermoplastic interlayers is that they can be made out of self-healing polymers, i.e. polymers which can restore their adhesive and internal strength autonomously or by a simple in-situ thermal treatment.

Within the field of self-healing polymer composites the majority of early studies focussed on extrinsic healing strategies in which an 'external' healing agent is added to the matrix prior to consolidation. The healing agent can be included via capsules, hollow fibres or vascular systems and is released upon fracture of the matrix [8-10]. The major drawback of these systems is that they only lead to single healing events and multiple healing (at a specific location) is not possible. In intrinsic healing polymer systems the restorative behaviour is embedded within the polymer structure itself and only needs an external trigger in the form of a modest temperature raise. Such polymers are theoretically capable of an infinite number of healing cycles [11,12], provided the healing conditions are such that the separated crack surfaces can come into contact again.

Ionomers are a class of thermoplastic polymers that are capable of intrinsic self-healing upon thermal activation as shown for scratch, ballistic impact and fatigue damage [13-17]. This healing takes place at modest temperatures, i.e. at around 100-120°C which is well below the overall melt flow temperature of the material. Hence, while being a thermoplastic, ionomers offer major advantages over conventional thermoplastic interlayer materials as damage repair does not require reheating to a high temperature at which massive flow

occurs everywhere in the structure. In the case of healing of ionomers the macroscopic flow is restricted to local areas around the damage or delamination site. Moreover, ionomers have also been employed as interlayer material in conventional carbon fibre/epoxy composites due to their good adhesive properties [5,18]. These two characteristics make ionomers ideal candidates to be used as self-healing interlaminar systems for CFRP structures.

However, as long as self-healing interface layers for CFRPs are in their development stage and the conditions of guaranteed quasi-autonomous repair are yet to be defined, there will be a need for NDT of delaminations and internal damage in a quantitative or at least semi-quantitative manner. The appropriate NDT techniques to monitor such damage should at least provide information on the areal extent of the damage and if possible on the location and height of the internal cavity. Although the requirement for non-destructive healing evaluation seems evident, the majority of studies that investigate the self-healing behaviour of composite materials focus on destructive testing of damaged and healed samples and the involvement of NDT is limited to a couple of studies only [19-24].

One of the most powerful NDT techniques for the detection of meso- and macroscopic damage in composite materials is the use of broad-band ultrasound, i.e. elastic waves with frequencies above 20 kHz. By appropriate analysis of the reflection or transmission of ultrasonic waves, several types of damage, such as voids, cracks and delaminations, can be detected and localized [25-29]. This approach has been thoroughly developed in the past, and is currently adapted for NDT in a number of industrial applications. A recent development in the field of ultrasonics is based on the occurrence of local defect resonance (LDR) [30,31]. In this testing mode, an internally damaged component is excited at such a frequency that the damage region is forced into a resonance vibration mode with local displacements being several times higher than its surroundings. This resonance signal is then detected and used to reconstruct and visualise the location and dimension of the damage site. Since the LDR vibration is constrained exclusively in the defect area, the spatial resolution of the resonant imaging is comparable with conventional ultrasonic NDT techniques despite the lower frequencies used.

In this work, a comparative study is performed on carbon fibre reinforced polymer (CFRP) composites with an ionomer interlayer in which artificial delaminations of various sizes and at different locations were introduced

during production. The dimensions of the defects prior and after thermal healing are measured by conventional ultrasonics and LDR. In addition, the compressive strength of the as- produced and healed samples is measured and the data are correlated to the various NDT results.

2. Material and methods

2.1. Materials

Prior to composite production, CFRP laminates of 1mm were produced by infusing two layers of satin woven carbon fibre fabrics (285g/m^2, Haufler composites) with Epikote^{TM} 04908 resin (HEXION). The CFRP layers were cured for 16 hours at room temperature and post-cured for 8 hours at 80°C, as prescribed by the resin supplier, resulting in laminates with a Tg of approximately 90°C. PV5414 ionomer films (500µm thickness) were obtained from DuPont®.

2.2. Ionomer-CFRP laminate production

Ionomer-CFRP laminates of 10x10 cm^2 were produced by stacking and two-step pressing the CFRP and ionomer components for 1 minute at 100°C with a pressure of 1 MPa using a hot press. The overall stacking sequence consists of 2 layers of CFRP and 2 layers of ionomer film. Artificial delaminations (i.e. non-fused regions) were introduced by placing two aluminium plates containing a circular hole of either 2 or 5 cm in between the heated dies of the hot press and the outer CFRP layers prior to the last pressing step. The size of the resulting non-fused areas, the delaminations, corresponds to the size of the hole within the aluminium plate. A schematic overview of the ionomer-CFRP laminate production is shown in Figure 1. For the CFRP-ionomer laminate configuration shown in Figure 1a, two identical pre-pressed and perfectly bonded substructures each consisting of 1 layer CFRP and one layer ionomer film (5 minutes at 100°C and 1 MPa of pressure) were used. Using this protocol a delamination was created within the thermoplastic interlayer (called the 'soft-soft delamination' hereafter). This type of delamination is to be regarded as an internal defect in the thermoplastic interlayer itself. For the CFRP-ionomer laminate shown in Figure 1b, the final pressing was done with a single CFRP plate on the one hand and a perfectly bonded CFRP plate–ionomer substructure consisting of 1 layer CFRP and two layers of ionomer film on the other hand. This way, a delamination is introduced at the interface of the CFRP and the ionomer interlayer (called the 'rigid-soft delamination' hereafter). This type of

delamination is to be regarded as a proper delamination between layers of different properties, being the thermoplastic interlayer and the CFRP face plate.

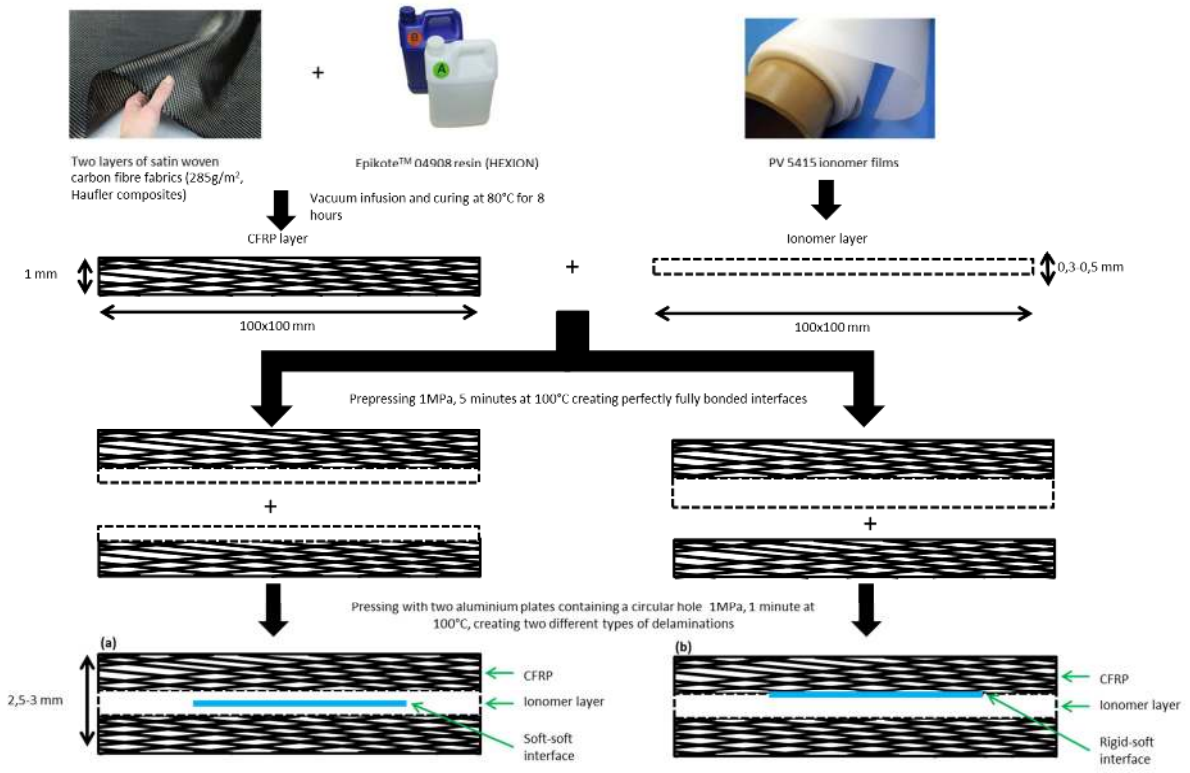

Figure 1 Schematic overview of the production process of the artificially induced delaminations in CFRP-ionomer laminates. Both the soft-soft (a) and rigid-soft (b) delamination production are shown.

2.3. Healing treatment

Healing was performed by pressure-less annealing of the laminates at a temperature of 100°C in a hot-air furnace. The specimens were healed for a total time up to 40 hours. However, to allow ultrasonic monitoring of the actual delaminated area during the annealing treatment, the specimens were taken out of the oven after 1, 2, 3, 4, 5, 6, 7, 8, 9, 10, 11, 12, 14, 16, 18, 20, 22, 24, 26, 28 and 40 hours for the water-coupled C-scan measurements and after 1, 2, 3, 5, 9, 11, 13, 15, 17, 20, 25 and 40 hours for air-coupled C-scan and LDR measurements. The NDT measurements were conducted at room temperature and typically took 30 minutes for the water-coupled C-scan measurements and 1 hour for the air-coupled C-scan and LDR measurements. No efforts were made to rapidly cool the samples from the oven temperature to room temperature. Although healing was performed above the Tg of both the epoxy and the ionomer, no thermal degradation of the polymeric phase was observed as is described in Supplementary information S1.

2.4. Characterization

2.4.1. Thermomechanical analysis of the ionomer film

The optimal healing temperature of the PV5414 ionomer film from a molecular mobility perspective was determined using a Perkin–Elmer Sapphire differential scanning calorimeter (DSC). Samples were heated and cooled between -50°C and 150°C at a rate of 20°C/min under a nitrogen atmosphere.

In order to obtain information on the flow characteristics of the PV5414 ionomer, the macroscale network mobility of the 500 µm film was investigated by small amplitude oscillatory shear rheology. The experiment was performed using a Haake Mars III rheometer, employing an 8 mm diameter (stainless steel) parallel plate geometry. A constant shear strain γ of 1% was applied, which is within the linear viscoelastic regime of the material. Frequency sweep experiments between 10^{2}–10^{-2} Hz were performed at temperatures of 70 and 100°C, with isothermal hold periods of 20 minutes in between temperature steps. The supramolecular bond lifetime (τ_b) at these temperatures was then calculated as the inverse of the frequency at which the storage and loss moduli crossover in a frequency sweep experiment [32].

2.4.2. Ultrasonic NDT analysis

2.4.2.1. Water-coupled ultrasonic C-scan experiments

Water-coupled C-scans, both in reflection and transmission, were made on the different samples and their various healing stages, in order to extract the remaining delaminated area and to quantify the progression of healing. Water temperature was measured to be 22°C ± 1°C. Dynamic time-gating, based on the pulse echo of the front surface, was applied for the C-scans in reflection. In this way, non-horizontality of the samples is compensated for and the imaging depth is kept constant. An ultrasonic pulse with a centre frequency f_c = 5 MHz was used (H5K transducer with diameter 13 mm, General Electric). The distance between transducer(s) and inspected sample was approximately 70 mm. The pulser/receiver apparatus operates at a sampling frequency of 400 MHz (USIP40, General Electric), and the maximum pulse amplitude is evaluated in the selected time gate. For both x-direction (index axis) and y-direction (scanning axis), a scan range of 0-120 mm was applied with a grid step of 1 mm and 0.1 mm respectively. The actual scanning speed was set at 50 mm/s.

2.4.2.2. Air-coupled ultrasonic C-scan experiments

Air-coupled C-scans were carried out after each heating step described in the healing protocol. The applied frequency was 200 kHz. The Ultran focused transducers (focus distance 38 mm, size of focus spot ~ 2mm) were positioned in a normal transmission mode. The transducers were powered with rectangular bursts of 200 V amplitude and 10 periods of carrier frequency. The data acquisition unit included 14-bit A/D converter with 5 MHz sampling frequency and 40 dB maximum amplification. In the C-scans, scanning steps of 1 mm along the x and the y-axes were combined with scanning speed of 20 mm/s along the x-axis.

2.4.2.3. LDR

Local Defect Resonance (LDR) is caused by a local decrease in stiffness for a certain mass of the material in direct contact with the area of delamination being in local resonance [31]. A frequency match between the input and the defect natural frequency results in a substantial increase in local vibrations which can be used for identification of the position and the size of the defect. The vibrations in the specimen were excited by piezo-actuators SI Scientific Instruments GmbH with a frequency response extended into high kHz range to comprise an expected value of LDR frequency of the delamination. To identify the LDR frequency the transducers are driven in chirp modes (bandwidth 200 kHz, input voltage 1-2 V) generated by the HP 33120A arbitrary waveform generator. The C-scan of the specimen surface was implemented with the laser vibrometer Polytec PSV 300 and colour coded images of the distributions of vibration amplitudes over the specimen surface were obtained for all resonance peaks in the vibration spectrum. The image with maximum vibrations localised inside the delamination area corresponds to its local resonance whose frequency and frequency response (amplitude vs. frequency) were identified from the spectrum data.

2.4.3 Mechanical characterization of the pristine and healed composites

In order to determine the effect of the delamination healing in the CFRP-ionomer composites on the in-plane compression strength the composites were mechanically loaded. Compression tests were performed using a well-aligned Zwick/Roell 250 kN universal testing machine with a crosshead speed of 1 mm/min. Samples were clamped on every side of the panel based on conditions as prescribed in ASTM D7137(M)-07. However, several amendments to the standard were made for practical reasons. As such, the dimensions of the specimen are selected differently, the clamping side plates have dimensions of 105 x 80 mm, a thickness of 5 mm and bolts were used per 30 mm clamping length. The non-delaminated specimen was tested 4 times. However, as all

delaminated and healed specimen had to be characterized by the various NDT techniques prior to mechanical testing, per condition only one sample was tested.

3. Results

3.1. Thermomechanical properties of the ionomer interlayer

Thermal characterization of the ionomer film was performed in order to obtain a good understanding of the healing characteristics of the ionomer interlayer prior to mechanical testing and non-destructive evaluation. The DSC curve in Figure 2 clearly shows the two main thermal transitions which are typical for ionomer based polymers. Both transitions play a specific role in the healing process [17].

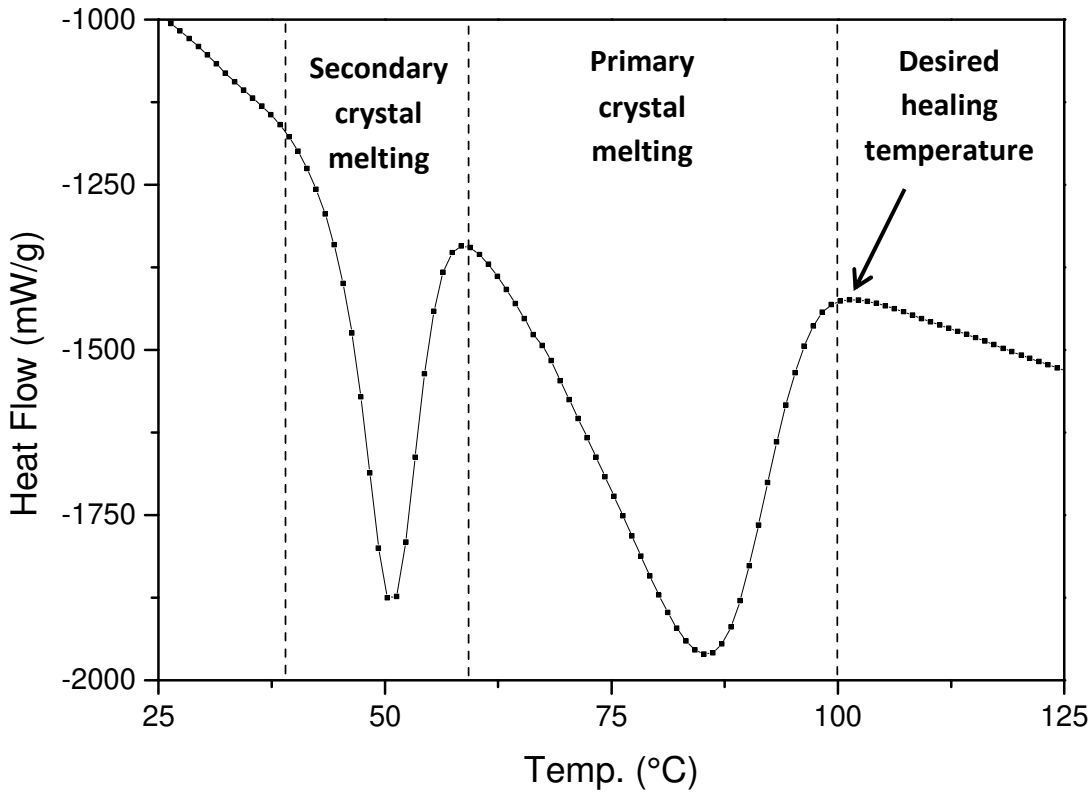

Figure 2 DSC curve of the heating of the ionomer interlayer. During heating, two healing stages can be identified, during which secondary and primary crystal melting occurs between 40-60°C and 60-100°C respectively.

Figure 2 shows that the primary polymer crystals melt at a temperature above 100°C. Previous work showed that full healing of the ionomer interlayers will only occur when annealed at or slightly above this temperature [17]. At these temperatures the polymer phase has enough mobility to flow locally while the ionic clusters maintain its rigidity preventing the polymer to flow at a macroscopic level. The critical temperature for healing based on DSC measurements is confirmed by the rheological data displayed in Figure 3 which show that the storage modulus G' and the loss modulus G" do not intersect at temperatures below 100°C. Hence, below this temperature, there is no macroscale mobility and therefore no healing.

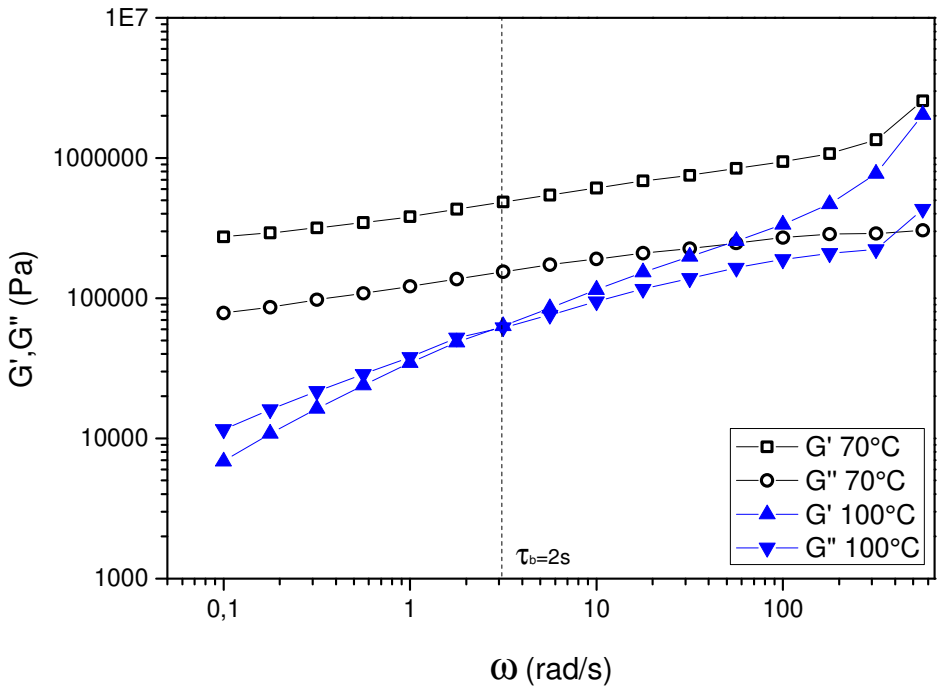

Figure 3 Frequency sweep experiment of the ionomer film at 70°C and 100°C. The supramolecular bond lifetime τ_b can be determined at the temperature were the storage and loss modulus intersect.

From the data in Figure 3, the supramolecular bond lifetime can be derived at the temperature where G' and G" intersect. For a healing temperature of 100°C, a τ_b of 2 seconds is determined ($\tau_b = 2\pi/\omega$). Since the plateau modulus that could be derived at this temperature exceeds 10^5 Pa, the used ionomer meets the semi-quantitative requirements for an intrinsic self-healing polymer combining good healing with decent mechanical properties [32].

3.2. Non-destructive characterization

3.2.1. C-scanning techniques

All delaminated CFRP-ionomer laminates prepared in this study were inspected before and after the full healing treatment by means of two implementations of C-scanning techniques: water-coupled (WCU) and air-coupled (ACU). The corresponding transmission images for the various laminated structures with a 5 cm and 2 cm delamination are displayed in Figure 4 and Figure 5 respectively. Using the WCU technique it is also possible to visualize the delaminations and healing using the reflection output. The reflection WCU scans are shown in the supplementary information (S1), where one can easily verify the complementarity between transmission and reflection WCU C-scans. Although the use of reflection over transmission is favourable from an application point of view, the transmission output is mainly analysed throughout this study in order to compare to the comparable transmission signal obtained in the ACU C-scans.

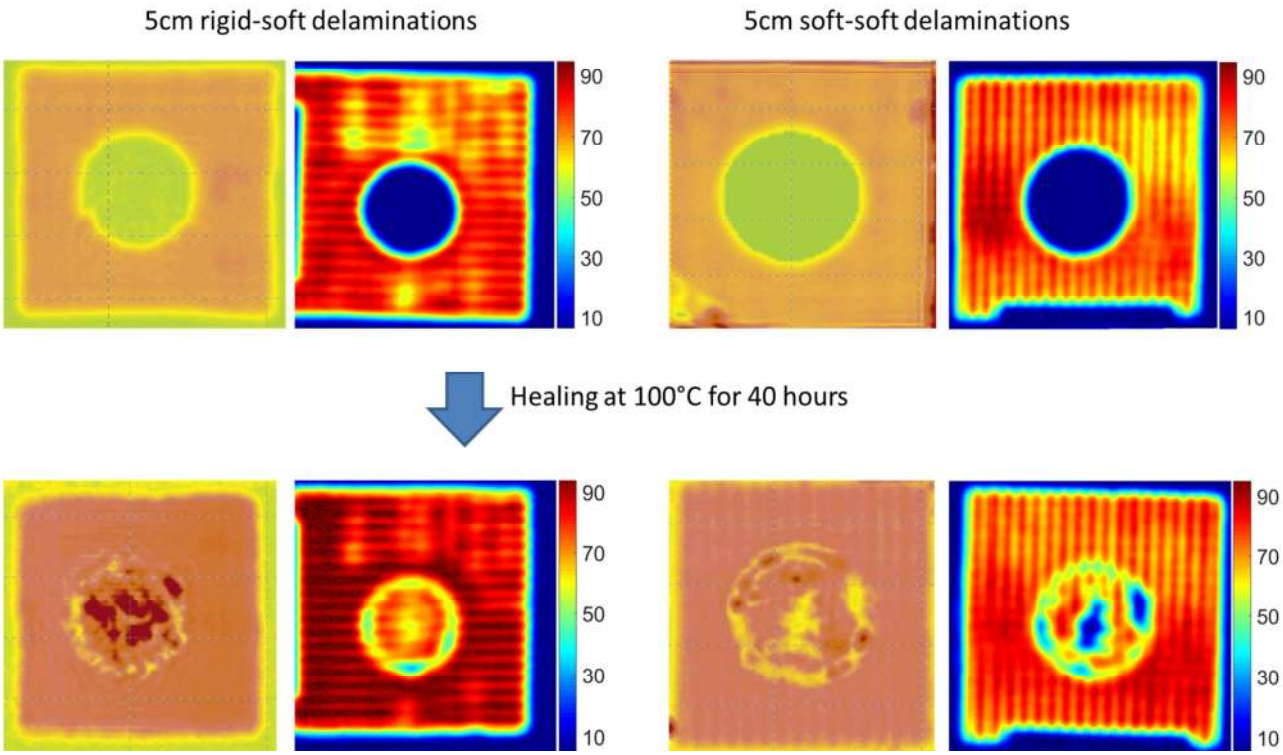

Figure 4 Overview of the C-scan transmission amplitude images for laminates with rigid-soft and soft-soft delamination with an initial radius of 5 cm scanned with ACU (left column) and WCU (right column). The top images clearly visualize the circular unhealed delaminations whereas the bottom images correspond to the scan results for the same specimen after a healing treatment at 100°C for 40 hours. Colour bar indicates percentage for WCU transmission.

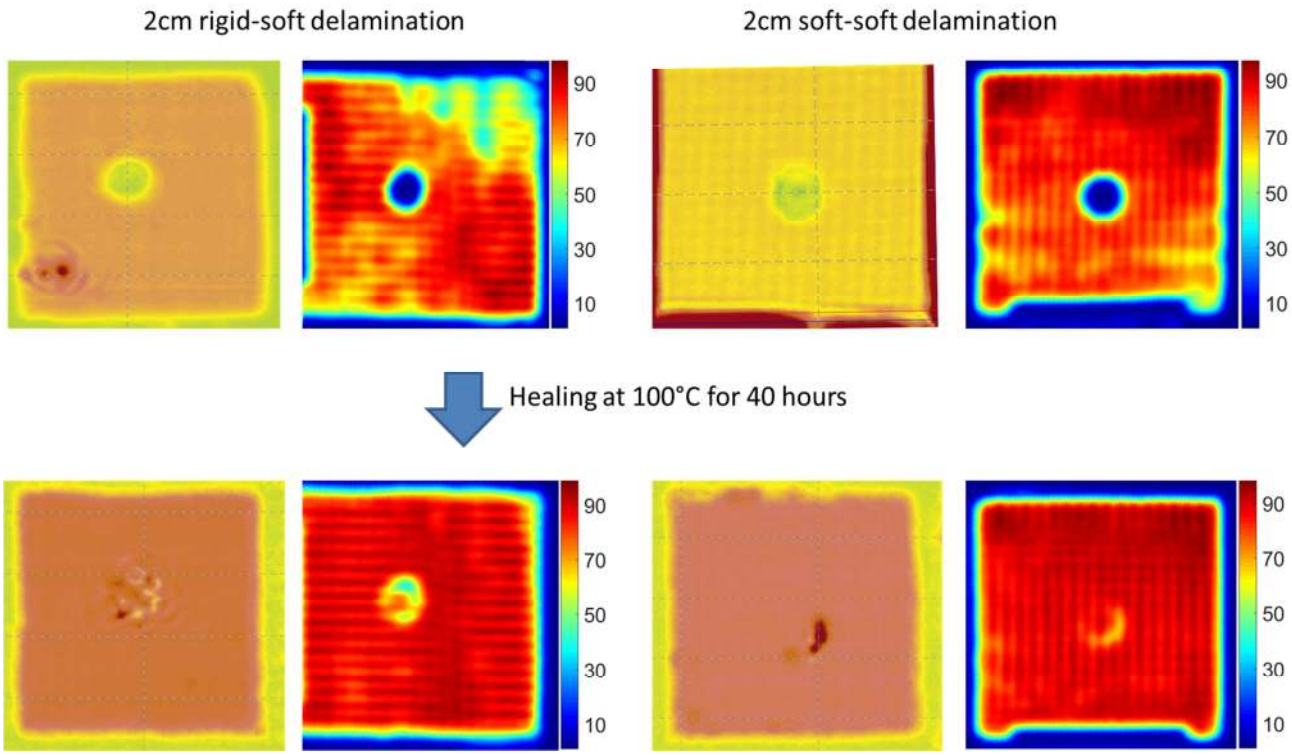

Figure 5 Overview of the C-scan transmission amplitude images for laminates with rigid-soft and soft-soft delaminations with an initial radius of 2 cm scanned with ACU (left column) and WCU (right column). The top images clearly visualize the circular unhealed delaminations whereas the bottom images correspond to the scan results for the same specimen after a healing treatment at 100°C for 40 hours. Colour bar indicates percentage for WCU transmission.

From the figures 4 and 5, it can be seen that both C-scanning techniques are equally capable of detecting the soft-soft and the rigid-soft delaminations. However, based on the scans, no distinction can be made between the two different types of delaminations. In addition, the scans also visualize the almost complete healing of the delaminations after healing for 40 hours at 100°C. Clearly, even in extensively healed specimens, traces of the original delaminated area can be detected.

For the 5 cm delaminations these traces are mainly located at the edges and in the middle of the original delaminations. The healed region in the rigid-soft specimen is more evenly distributed than that of the soft-soft specimen in which a more random distribution of the healed area is present. The unhealed zones at the edge of the delamination are believed to be caused by volumes of air that are trapped within the specimen upon production. In delaminations induced by low-velocity impact, pockets of trapped air will not be present, and therefore it is expected that such unhealed regions will not exist in actual applications. The unhealed zone in the middle of the specimen could be of similar origin but might also be caused by the fact that the delaminated

interfaces were too far apart initially and did not make contact during the non-pressurized healing treatment. The C-scan images for the 2 cm delamination specimen also show unhealed regions at the edge of the delamination. However, the middle regions seem to be fully healed in these specimens.

When comparing the WCU and ACU scans, it can be observed that the WCU scans clearly reveal the primary orientation of the carbon fibre fabric that is used whereas this hidden feature is less obvious in the ACU scans, which is a logical effect of the substantially lower frequency of the ACU scans (200 kHz vs 5 MHz). More interestingly, the ACU scans show a couple of darker regions within the healed areas which are not readily observed in the WCU scans. These regions indicate that the amplitudes of the transmitted waves through the healed areas are larger than those transmitted through the pristine areas. The higher transmission indicates additional acoustic matching in those areas which apparently caused by variation of local thickness of the ionomer layer and/or acoustic impedance of the healed interface. This implies that the nature of the healed region is somewhat different from that of the pristine regions.

In order to obtain further information on the healing mechanism of these delaminations, the specimens were monitored at intermediate steps during the entire healing process using WCU (soft-soft delaminations) and ACU/LDR (rigid-soft) delaminations. As an example, the healing of the 5 cm soft-soft delamination and of the 5cm rigid-soft delamination is shown in Figure 6 and Figure 7 respectively.

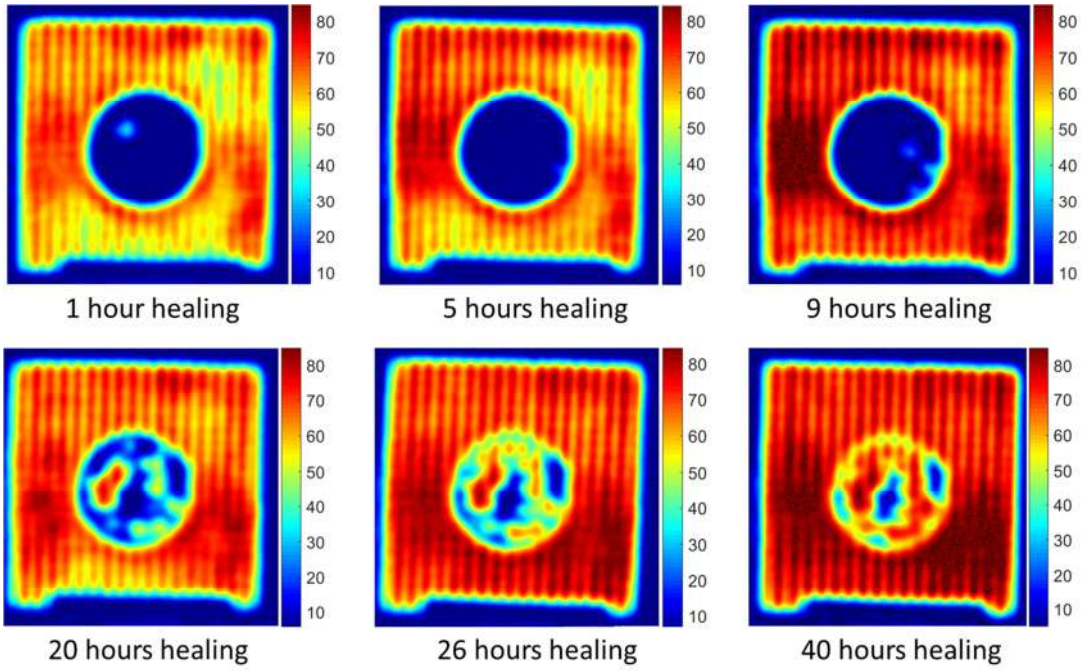

Figure 6 Healing of the 5cm soft-soft delaminated CFRP-ionomer laminate over time, monitored with WCU transmission C-scan. Healing is performed at 100°C. Accumulated healing time is indicated below each image. Colour scales indicate level of WCU transmission.

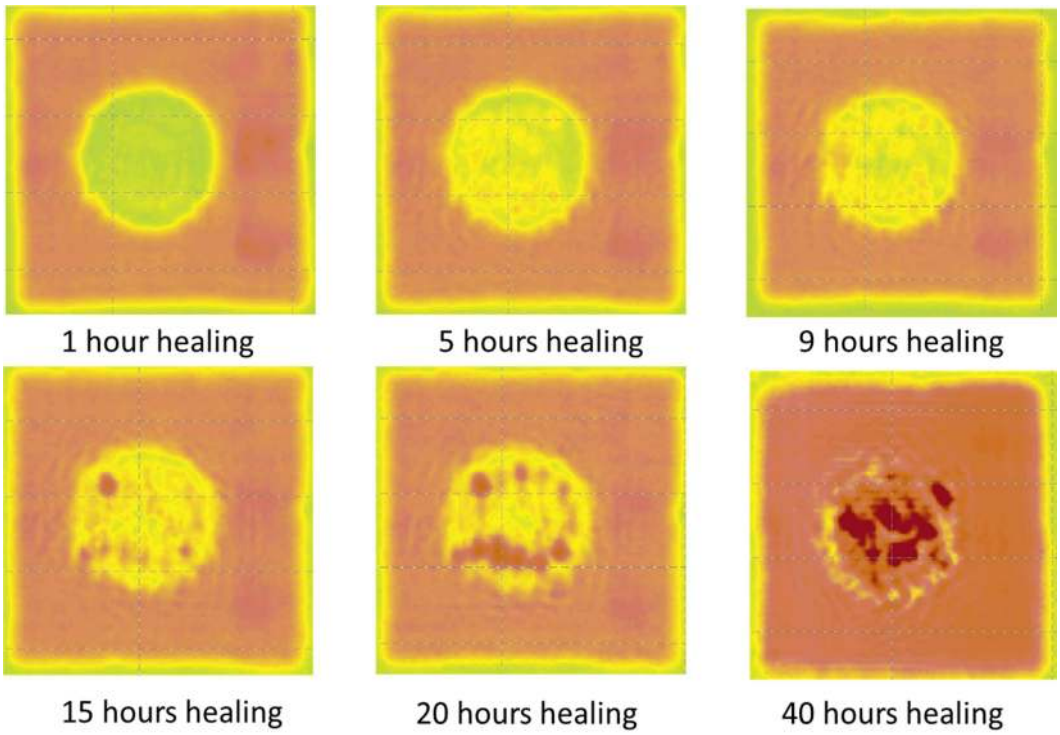

Figure 7 Healing of the 5cm rigid-soft delaminated CFRP-ionomer laminate over time, monitored with ACU scanning. Healing is performed at 100°C. Accumulated healing time is indicated below each image.

Figure 6 and Figure 7 show that the healing in the soft-soft and rigid-soft specimens becomes visible after 9 and 5 hours respectively. However, these relatively long onset times are mainly attributed to the fact that in the initial stages of the experiment, the specimen has more frequently been scanned and therefore removed from the oven. For this reason, it can be expected that in a continuous healing scan the onset of perceptible healing would occur at an earlier stage. Furthermore, it is observed that the healing process within the delamination starts from small nucleation points which then grow into bigger regions that ultimately merge together into the healed areas presented in Figure 4. Similar nucleation and growth events were also observed for all other delamination types covered in this study.

In Figure 8 we plot the normalised delaminated area as a function of the accumulated healing time at 100°C for both the 5 cm and the 2 cm diameter initial delaminations for the soft-soft composites, as determined by the WCU transmission C-scanning. To quantify the healing , after each healing step, the total area in the delaminated zone was determined for which the transmission amplitude was larger than 60% (relative to the intact region). The figure shows that there is a certain minimal healing time before the healing becomes detectable and that this minimal time is longer for the larger diameter delamination. Furthermore, the figure shows that in both cases the healing at the longest annealing times has not led to complete disappearance of the delamination as some ultrasonic scattering centres remain at the delamination site. It should be pointed that, given the manner in which the delaminations were introduced, these scattering centres are unlikely to be due to filament fracture but rather correspond to remaining imperfections at the healed interfaces.

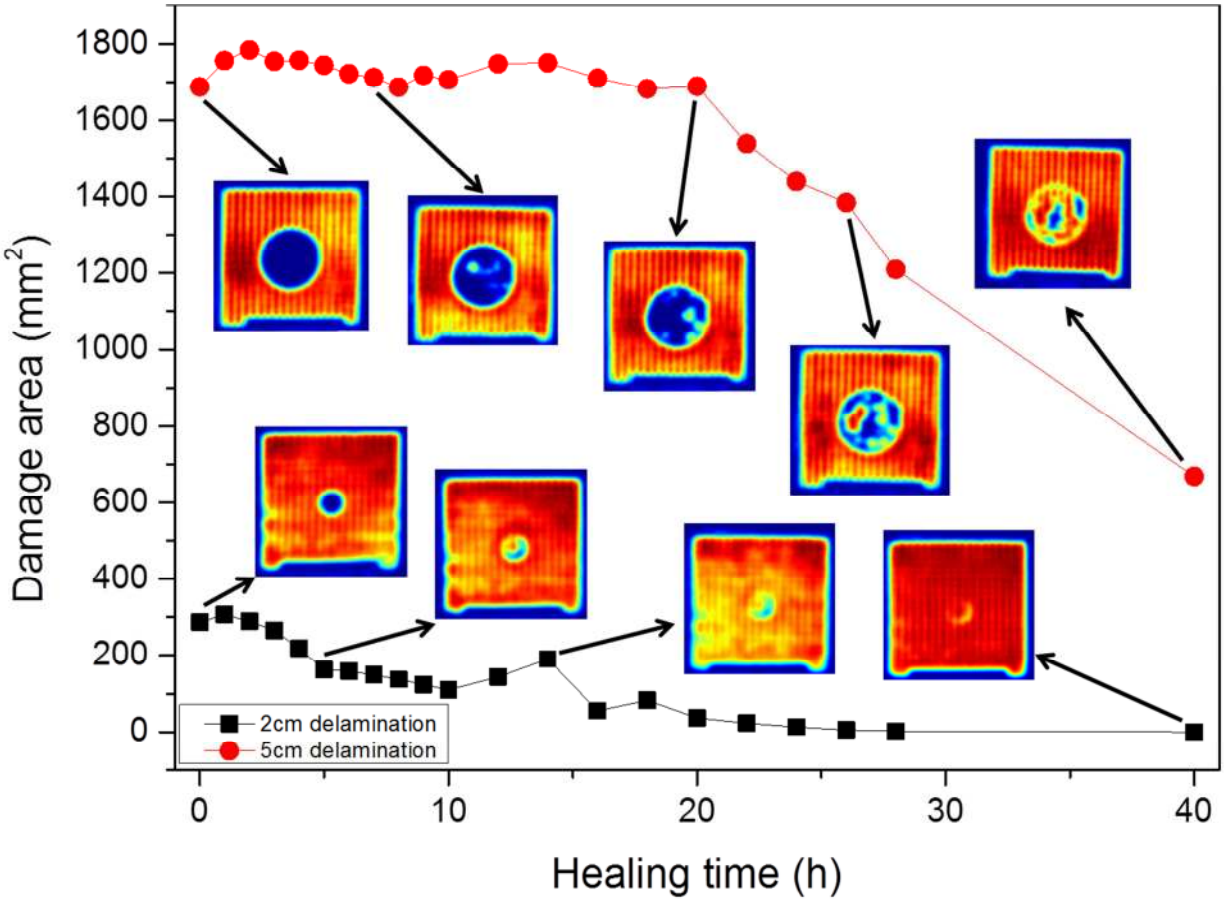

Figure 8 Delaminated area as function of the accumulated healing time at 100 °C for both the 5 cm and the 2 cm diameter initial delaminations for the soft-soft composites, as determined by WCU.

3.2.2. Local defect resonance scanning

Figure 9 shows the evolution of the local defect resonance (LDR) of a composite with a 5 cm delamination induced at the rigid-soft interface during several stages of the healing treatment. Clearly, both the frequency response and the amplitude of the LDR signal change as healing progresses.

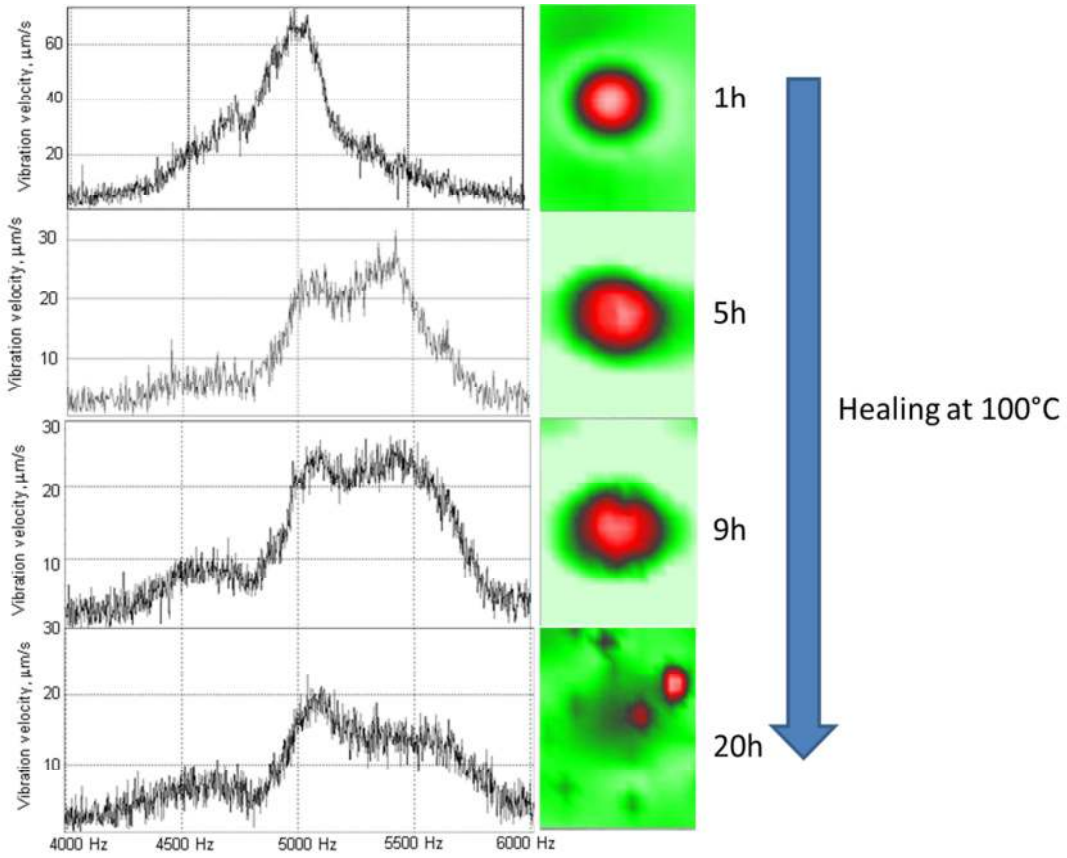

Figure 9 Evolution of the LDR response of a CFRP-ionomer composite with a 5cm delaminations induced in the rigid-soft interface over a 20 hour healing treatment at 100°C.

Figure 9 shows that the centre of the delamination frequency response shifts to the higher values as a function of healing time. This frequency variation is plotted in Figure 10 and exhibits a dramatic shift in the first few hours of the heating. The data in this figure enable to clarify the structure of the delamination resonance and some features of the healing process. The LDR frequency value for circular delaminations (and the defects like flat-bottomed holes (FBH)) is described by the following formula [31]:

$$f_0 \approx \frac{1.6h}{R^2}\sqrt{\frac{E}{12\rho(1-v^2)}} \qquad (1)$$

where h is the thickness of the vibrating component in the composite and R is the radius of the defect. For an isotropic CFRP fabric, an in-plane Young's modulus E of 60 GPa, a material density ρ of $6 \cdot 10^3$kg/m^3 and a Poisson^s ratio v of 0.1 can be estimated. By using $h = 1$mm for the CFRP layer and $R = 2.5$ cm for the delaminated area in the above relation a f_0 of approximately 4500 Hz is obtained for the unhealed situation which is in very close agreement with the measurement in Figure 10, even though the properties of the tested

laminates are not fully isotropic. The agreement indicates that the LDR signal is due resonant vibrations of the unloaded (delaminated) part of upper CFRP layer in the rigid-soft configuration (Figure 1).

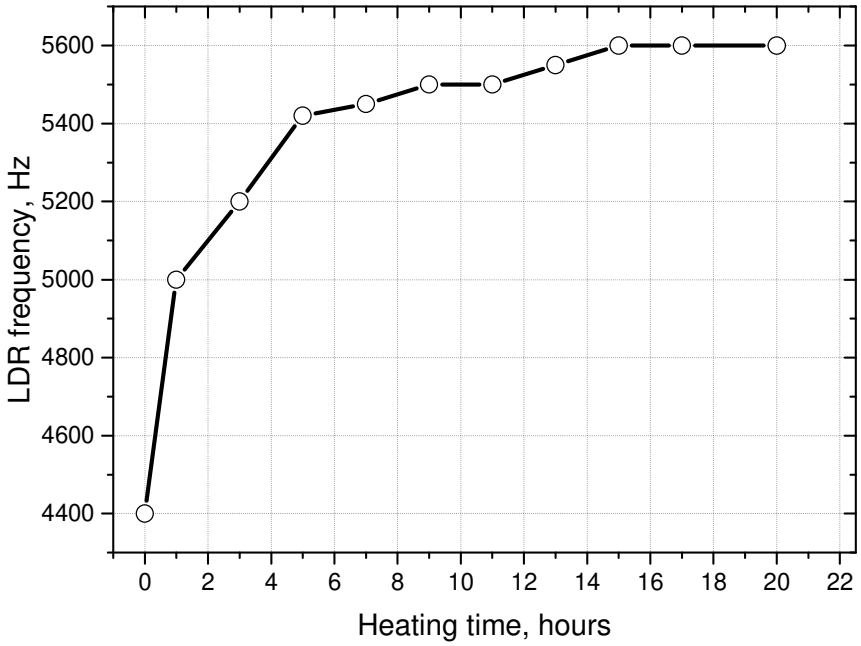

Figure 10 Evolution of the LDR frequency of the 5cm rigid-soft delaminated specimen as function of the healing time

Another feature seen in the plots of Figure 9 is related to the decrease in amplitude and widening of the LDR response. This is an indication of the increase in damping of the resonant vibrations in the delamination area. Like in the case of a classical resonance, the quality factor Q of LDR is reciprocal to the energy loss of vibrations. An obvious decrease in Q on the course of self-healing in Figure 9 delivers the information on the reduced delaminated area and the through thickness gap closure at the delamination interface which must clearly cause the observed increase in vibration damping.

Despite the fact that the determination of LDR characteristics seems to be a good approach for quantification of the healing of the soft-rigid delamination, it appeared that no distinctive resonant behaviour could be detected for soft-soft delaminated specimens. The absence of a LDR response for these specimens follows from the mechanism of the delamination resonance clarified above: the internal surface of the CFRP layer which used to vibrate freely (like in a FBH) and resonate for the rigid-soft interface is clamped by an ionomer layer that prevents development of LDR in soft-soft interface.

3.3 Destructive characterization by compression testing

Compression test experiments were performed on pristine, delaminated and healed specimen (see section 2.2) to show the effect of damage and healing on the mechanical properties of the composites. As an example of the typical outcome of these tests, the resulting compression test curves for the soft-soft 5 cm delaminated specimen are shown in Figure 11. In this particular case, the healed sample had received an un-interrupted healing treatment at 100°C up to 40 hours.

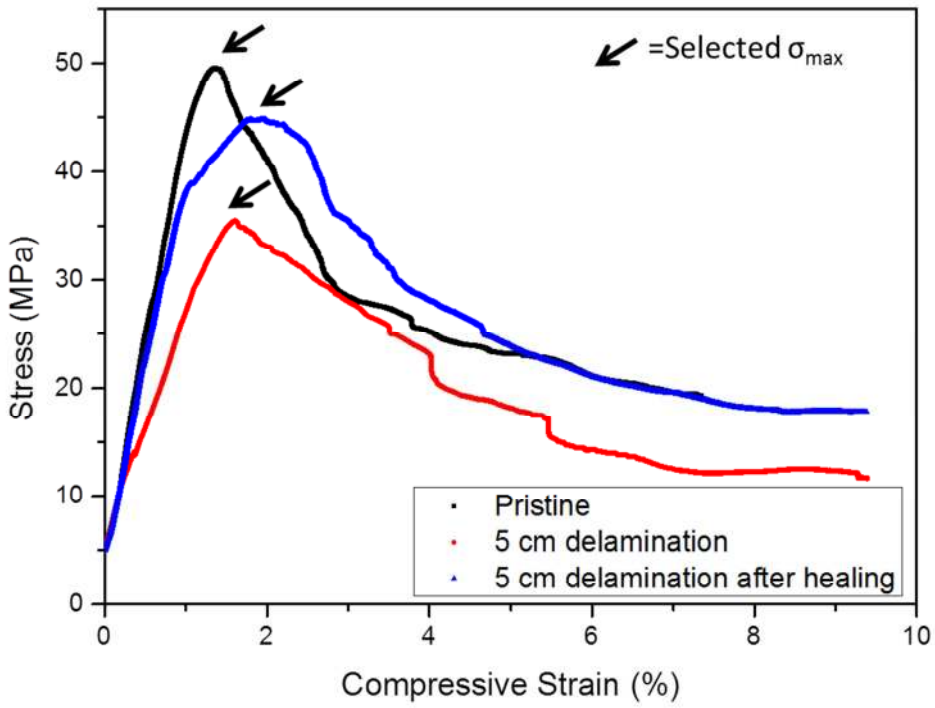

Figure 11 Compression test curves for the 5 cm soft-soft CFRP-ionomer composite. Partial restoration of the compressive strength is shown after 40 hours of healing.

From Figure 11, it is clear that the introduction of a delamination within the thermoplastic layer leads to a definite lowering of the compressive strength. After healing, an increase in the ultimate compressive strength is observed although the value of the undamaged specimen is not fully recovered. Similar trends were observed for all other laminated composites, and their compressive strengths are listed in Table 1.

Table 1 Overview of the ultimate compressive strengths of delaminated and healed CFRP-ionomer laminates (40 hours of healing with intermittent stops)

Initial delamination size	**Ultimate Compressive Strength (MPa)**			
	Soft-soft		*Rigid-soft*	
	Non-healed	*Healed*	*Non-healed*	*Healed*
2cm	48.0	47.2	42.2	45.5
5cm	35.5	44.8	41.1	47.1

4. Discussion

While the healing of damage (cracks and delaminations) in bulk ionomer samples [13,15,33] and particulate composites with ionomers as the matrix polymer [16,17,34] has been reported extensively in the literature, the current observations show for the first time the healing of delamination damage in CFRP composites with ionomer as the thermoplastic interlayer. The reduction of the delamination sites has been monitored using three non-destructive inspection techniques and the post-healing compression experiments demonstrated that the reduction of the delamination zone was accompanied by an increase in the compression strength, i.e. by restoration of the local adhesion and hence the overall load bearing capability.

We will now look in more detail into the actual reduction of the delamination sites as a result of the intrinsic self-healing nature of the ionomer. In many self-healing polymer systems the so called ‘zipper mechanism’, in which a local healing event automatically creates the surface contact for the subsequent healing step, is found to be the key factor to facilitate healing [35-37]. It is reasonable to expect that such a mechanism, starting from the edges of the delaminations, also might hold for the closure of the artificial delaminations. Figure 6 and 7 show that the healing grows not only from the edges but also from any point of cross-interface contact created

during the annealing. It is likely that an assumed discontinuous curvature in the ionomer layer as a result of the compression stress that is applied on the edges of the polymer film during the laminate production process, is responsible for the slower healing from the edges and the presence of a weak residual 'rim' in the ultrasonic images for the samples healed for the longest healing time is due to this effect. The discontinuous curvature of the ionomer at the edges of the delamination would also explain the observed incubation time for healing (Figure 8). If this explanation is valid, it may imply that 'real' delaminated surfaces (e.g. from low-velocity impact loading) would not suffer from this effect, and that such delaminations might follow the expected healing direction from the edges towards the middle. Another explanation for the incomplete healing as observed in figures 5-10 might be related to the thermal method used to create the delamination area leading to the presence of entrapped air in the zone of controlled non-fusion. As after production the delamination is surrounded by fully dense material and ionomers are almost impermeable to air, the contraction of the delamination would lead to 'bubbles of slightly compressed trapped air' which would prevent full healing as the opposing sites of such bubbles would never get in contact and hence such bubbles would never heal (certainly not in the case of healing in the absence of an external contact reinforcing pressure). An indirect indication for the role of trapped air in determining the final state after complete healing comes from an additional experiment that was performed on an 'open' soft-soft delamination for which the resulting WCU scan images are displayed in Figure 12.

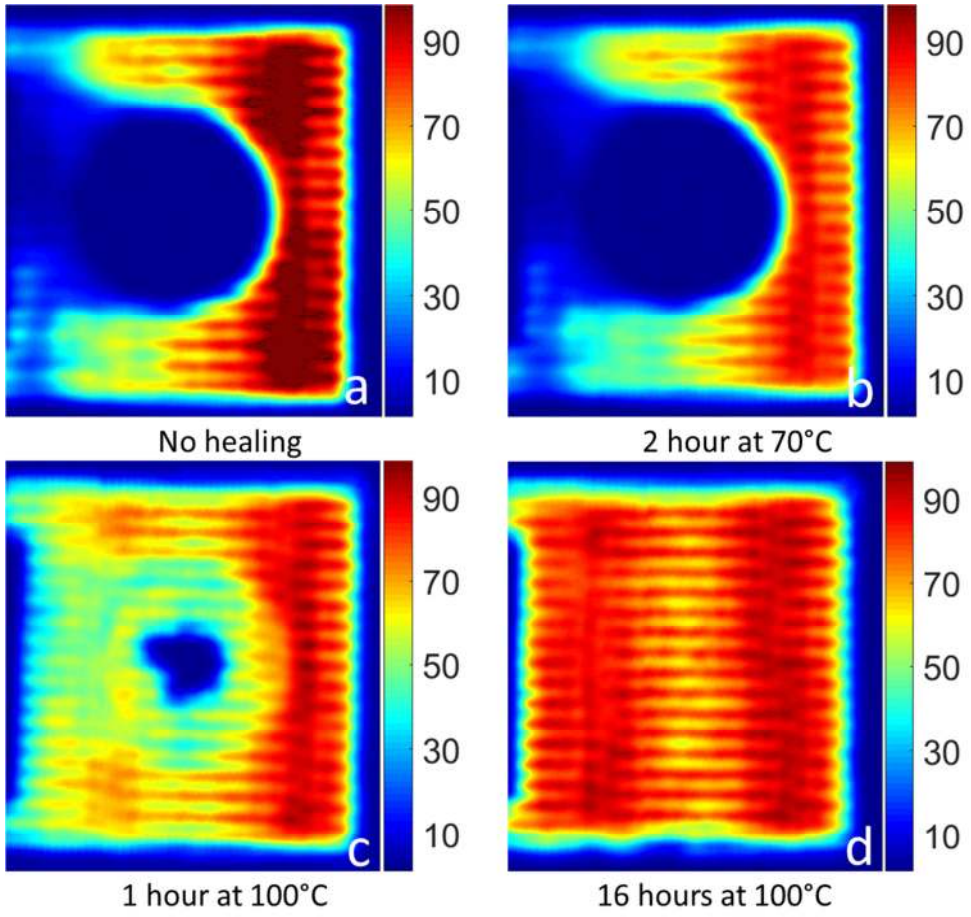

Figure 12 WCU scan of a soft-soft delamination that is open on one side. The specimen was scanned using WCU during different stages of the healing process. Color scale indicates the level of transmission.

The WCU scans initially show one open side of the delamination which is in contact with the surrounding environment (Figure 12a). Subfigure 12b supports the thermomechanical conditions for effective healing discussed above and confirms the absence of healing after a treatment at 70°C, i.e. below the minimal healing temperature as defined from DSC and rheometry. More interestingly, Figure 12c shows very progressive healing after only 1 hour of healing at 100°C compared to the closed delamination in Figure 6. Additionally, the delamination seems to close from the edges towards the middle following the zipper mechanism, and the delamination appears to be fully closed after 16 hours of healing. Hence full interfacial healing might be obtainable for ionomer interlayers in CFRP composites under the right conditions.

While the three ultrasonic techniques (ACU, WCU and LDR) give more or less the same type of information regarding the healing of the delaminations there are also some interesting differences. The plot of the LDR frequency during healing clearly demonstrates the growth of multiple zones within the delaminated zone as

the LDR spectrum changes from a single frequency peak to a wider spectral frequency response as is shown in Figure 9. However, the LDR analysis does not provide the all-inclusive information on the shape of the delamination as the employed C-scanning techniques do. On the other hand, Figure 10 and 11 clearly show that both the drop of the vibration amplitude and the shift of the LDR frequency undergo the largest transition during the onset of the healing, as opposed to the C-scanning techniques in which the healing effect becomes most prominent at the end of the process as explained previously. Neither WCU nor ACU showed noticeable sensitivity to these nucleation points which implies that the LDR based non-destructive technique is capable of monitoring healing events at an earlier stage than the ultrasonic C-scanning techniques, provided the mechanical quality factor of at least on the damaged interfaces is high enough to be detected.

Finally, we like to demonstrate that the observed reduction of the delamination area as determined by ultrasound techniques is not because the delamination area has dropped below the resolution limit for ultrasound but indeed is accompanied by a recovery of the adhesion force and hence the mechanical strength as determined in in-plane compression tests. To this aim we plot in Figure 13 the compression strength (i.e. the maximum load in the compression test) against the delaminated area as determined by WCU. The plot contains data points for defect free composites, as-produced composites with small and large delaminations and composites healed for 40 hours at 100°C, i.e. fully or partially healed samples. The data plotted in Figure 13 clearly demonstrate that healing not only leads to a reduction in delaminated area but also to an increase in compression strength. Furthermore, within experimental uncertainty all data points seem to lie more or less on a single line connecting compression strength to delaminated area, i.e. there is not much difference between the strength of a pristine composite with an artificial as-produced delaminated area and that of a composite with a healed delamination of the same area. The observed trend is in accordance with the well-known strength to delaminated area after impact relation[38-41]. Finally, the extrapolated strength for a fully healed delaminated sample corresponds to that of the perfect pristine sample, which indicated that the remaining interfacial imperfections as determined by the ultrasonic tests are relatively harmless from a mechanical point of view.

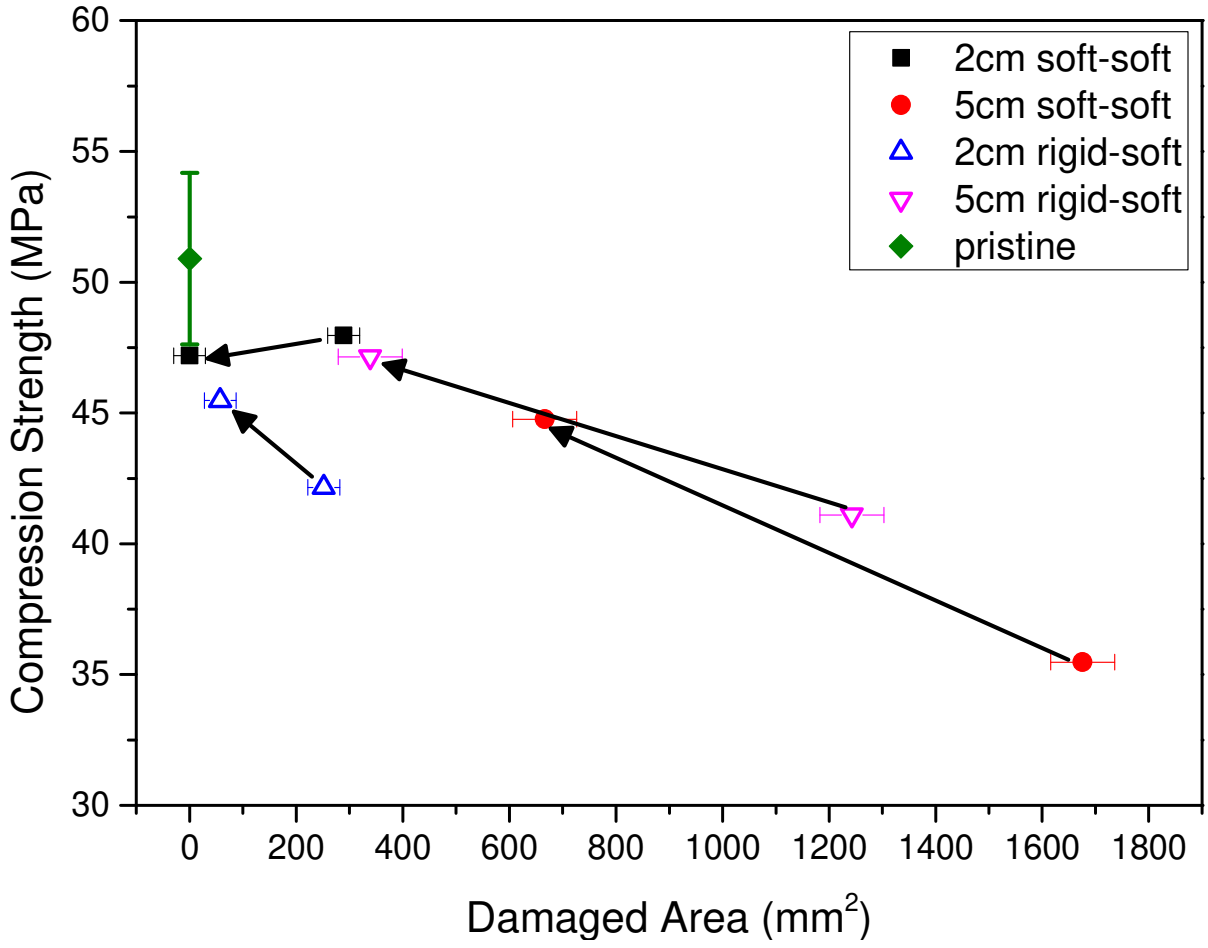

Figure 13 Relation between the compression strength and the delaminated area for the CFRP-ionomer composites tested. Results prior to thermal healing and after the full sequence of healing steps are shown for two different types of delaminations and two different initial sizes. Arrows indicate the effect of the thermal healing treatment (40 hours at 100°C, with intermittent stops). Error bars for delaminated area were estimated based on the error found in the WCU scans before the onset of healing.

5. Conclusion

The healing of artificial delaminations in CFRP composites with an ionomer interlayer is demonstrated by both air-coupled ultrasonic (ACU) and water-coupled ultrasonic (WCU) C-scan methods. Delaminations were introduced either within the ionomer layer (soft-soft interface) or at the CFRP-ionomer interface (rigid-soft interface). Both ACU and WCU show that healing starts from local nucleation points which then grow into larger zones of healed area. The ACU and WCU images were more informative at the final stages of the healing

process. Using a Local Defect Resonance (LDR) approach early stages of healing could also be detected and monitored. For the ACU and the WCU method, no differences were detected between the soft-soft and rigid-soft delaminations, whereas LDR analysis distinguished between rigid-soft delaminations (detectable) and soft-soft delaminations (undetectable). Finally, it was shown that for large delaminations, a quasi-linear relation was found between the delaminated area measured with C-scanning and the failure strength in compression for both pristine and partially healed samples. The communality in the correlation indicates that the contribution of the healed delamination to the compression strength equals that of the pristine interlayer.

Acknowledgements

The authors gratefully acknowledge funding from the European Union's Seventh Framework Programme under grant agreement number 314768. Mathias Kersemans acknowledges the financial support of Bijzonder Onderzoeks Fonds BOF (grant BOF.PDO.2015.0028.01).

Supplementary information S1: Thermogravimetric analysis of laminate components

Thermogravimetric analysis was performed to investigate the thermal stability of the composite components using a TG/DTA-7 Pyris Diamond (PerkinElmer). Figure S 1a shows a temperature ramp of 10°C/min for the ionomer-CFRP laminate components. From this figure it is clear that all laminate components have a degradation temperature (2% weight loss) well above 300°C thereby indicating the thermal stability at the applied healing temperature (100°C). To add to this statement, Figure S 1b shows an isothermal treatment of the CFRP laminate at 100°C for 60 hours without any measurable thermal degradation. In addition, differential scanning calorimetry (DSC) was performed using a Perkin–Elmer Sapphire differential DSC. Samples were heated and cooled between -50°C and 200°C at a rate of 10 °C/min under a nitrogen atmosphere. Figure S 2 shows the two thermograms of the CFRP interlayer before and after a thermal treatment of 60 hours at 100°C. No distinct differences that could indicate any form of thermal degradation were observed in these thermograms.

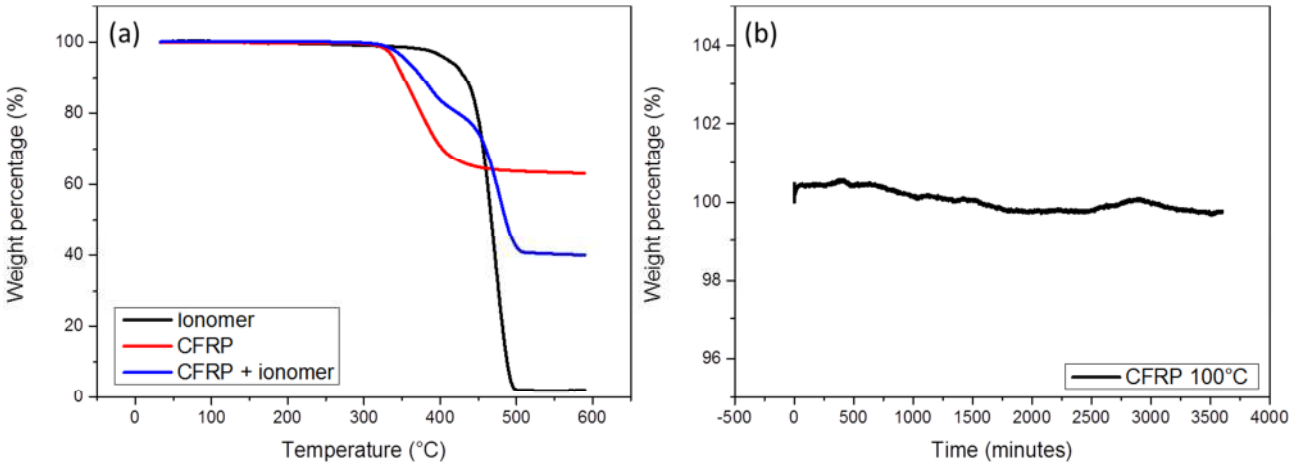

Figure S 1TGA temperature ramp of the individual components of the CFRP-ionomer composite (a) and the residual weight of the CFRP during an isothermal treatment of 100°C.

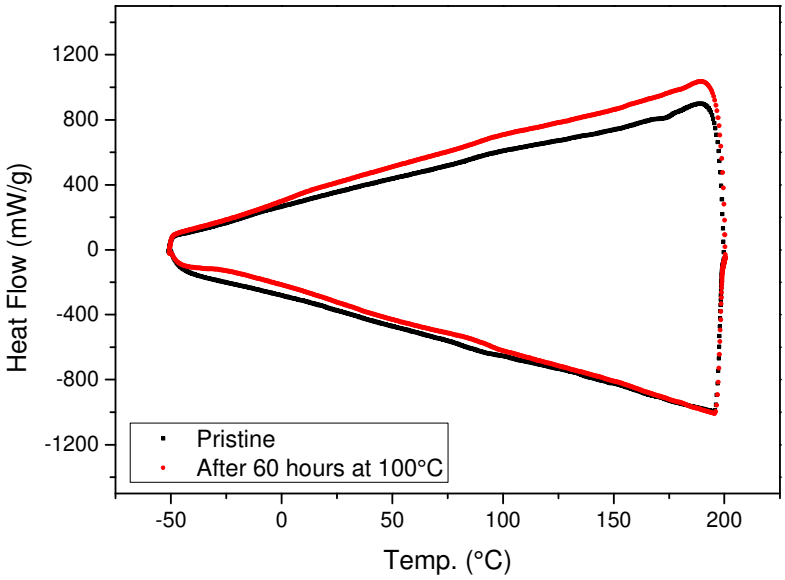

Figure S 2 DSC thermogram of the CFRP laminate layer before and after a thermal treatment of 60 hours at 100°C.

Supplementary information S2: WCU reflection scans

Figure S 3 shows the healing of both rigid-soft and soft-soft delaminations with an initial radius of 5cm visualized by WCU reflections scans.

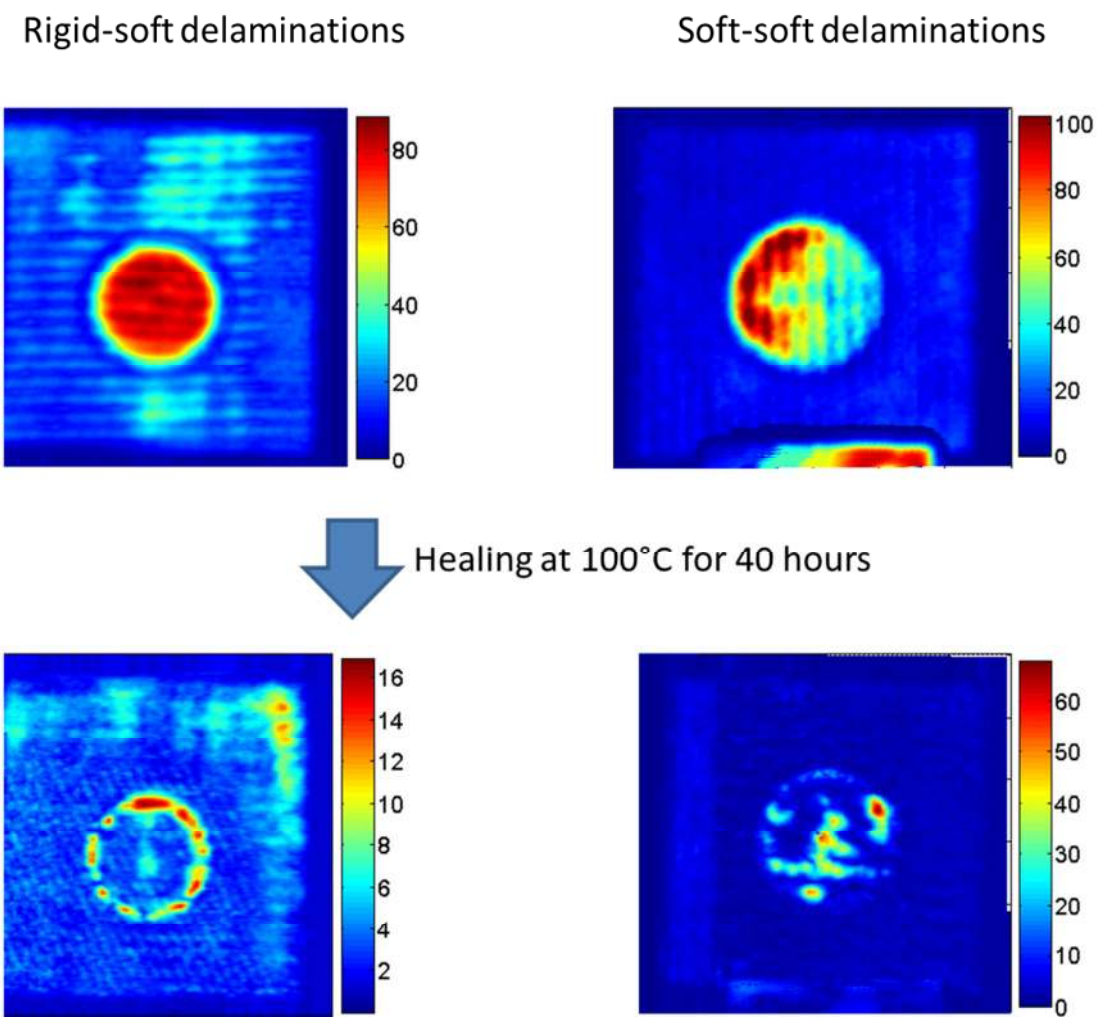

Figure S 3 Overview of the WCU-scan reflection amplitude images for laminates with rigid-soft and soft-soft delaminations with an initial radius of 5 cm). The top images clearly visualize the circular unhealed delaminations whereas the bottom images correspond to the scan results for the same specimen after a healing treatment at 100°C for more than 40 hours. Colour scales indicate level of WCU reflection.

Supplementary information S3: Healing efficiencies

The healing efficiency for the ultimate tensile strength (UTS) was determined by comparing the healed strength values to those of the largest damaged site measured (in this case the 5 cm soft-soft specimen) by:

$$UTS\ efficiency = \frac{\sigma_{healed} - \sigma_{largest\ damage}}{\sigma_{pristine} - \sigma_{largest\ damage}} \quad \text{(S1)}$$

The NDT healing efficiency of the area (A) measured by water coupled ultrasound (WCU) C-scanning measurement was calculated by:

$$NDT\ efficiency = 1 - \frac{A_{healed}}{A_{damaged}} \quad \text{(S2)}$$

The UTS and NDT healing efficiencies are plotted versus each other for the four specimen investigated in this study in Figure S 4

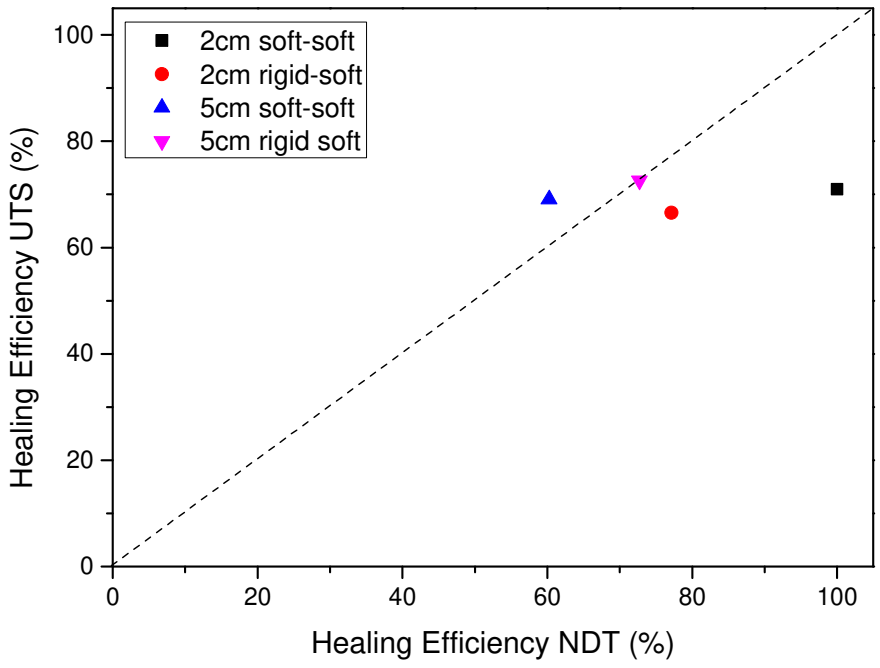

Figure S 4 Calculated healing efficiency of the ultimate tensile strenght vs. the healing efficiency determined by non-destructive WCU testing.

References

1. Chung, D.D.L. *Composite materials*. 2nd ed.; Springer London: 2010.
2. Agarwal, B.D.; Broutman, L.J.; Chandrashekhara, K. *Analysis and performance of fiber composites*. Third Edition ed.; John Wiley & Sons: 2006.
3. Agrawal, S.; Singh, K.K.; Sarkar, P.K. Impact damage on fibre-reinforced polymer matrix composite - a review. *Journal of Composite Materials* **2014**, *48*, 317-332.
4. Norris, C.J.; Bond, I.P.; Trask, R.S. The role of embedded bioinspired vasculature on damage formation in self-healing carbon fibre reinforced composites. *Composites Part A: Applied Science and Manufacturing* **2011**, *42*, 639-648.
5. Hojo, M.; Matsuda, S.; Tanaka, M.; Ochiai, S.; Murakami, A. Mode i delamination fatigue properties of interlayer-toughened cf/epoxy laminates. *Composites Science and Technology* **2006**, *66*, 665-675.
6. Greenhalgh, E.; Hiley, M. The assessment of novel materials and processes for the impact tolerant design of stiffened composite aerospace structures. *Composites Part A: Applied Science and Manufacturing* **2003**, *34*, 151-161.
7. Yasaee, M.; Killock, C.; Hartley, J.; Bond, I.P. Control of compressive fatigue delamination propagation of impact damaged composites using discrete thermoplastic interleaves. *Applied Composite Materials* **2015**, *22*, 559-572.
8. White, S.R.; Moore, J.S.; Sottos, N.R.; Krull, B.P.; Santa Cruz, W.A.; Gergely, R.C.R. Restoration of large damage volumes in polymers. *Science* **2014**, *344*, 620-623.
9. Luterbacher, R.; Trask, R.S.; Bond, I.P. Static and fatigue tensile properties of cross-ply laminates containing vascules for self-healing applications. *Smart Materials and Structures* **2015**, *25*, 015003.
10. Toohey, K.S.; Hansen, C.J.; Lewis, J.A.; White, S.R.; Sottos, N.R. Delivery of two-part self-healing chemistry via microvascular networks. *Advanced Functional Materials* **2009**, *19*, 1399-1405.
11. Zhong, N.; Post, W. Self-repair of structural and functional composites with intrinsically self-healing polymer matrices: A review. *Composites Part A: Applied Science and Manufacturing* **2015**, *69*, 226-239.
12. Garcia, S.J. Effect of polymer architecture on the intrinsic self-healing character of polymers. *European Polymer Journal* **2014**, *53*, 118-125.
13. Kalista, S.J.; Pflug, J.R.; Varley, R.J. Effect of ionic content on ballistic self-healing in emaa copolymers and ionomers. *Polymer Chemistry* **2013**, *4*, 4910-4926.
14. Varley, R.J.; Shen, S.; van der Zwaag, S. The effect of cluster plasticisation on the self healing behaviour of ionomers. *Polymer* **2010**, *51*, 679-686.
15. Vega, J.M.; Grande, A.M.; van der Zwaag, S.; Garcia, S.J. On the role of free carboxylic groups and cluster conformation on the surface scratch healing behaviour of ionomers. *European Polymer Journal* **2014**, *57*, 121-126.
16. James, N.K.; Lafont, U.; van der Zwaag, S.; Groen, W.A. Piezoelectric and mechanical properties of fatigue resistant, self healing pzt-ionomer composites. *Smart Materials and Structures* **2014**, *23*, 055001
17. Post, W.; Bose, R.; García, S.; van der Zwaag, S. Healing of early stage fatigue damage in ionomer/fe3o4 nanoparticle composites. *Polymers* **2016**, *8*, 436.
18. Wang, C.H.; Sidhu, K.; Yang, T.; Zhang, J.; Shanks, R. Interlayer self-healing and toughening of carbon fibre/epoxy composites using copolymer films. *Composites Part A: Applied Science and Manufacturing* **2012**, *43*, 512-518.
19. Prajer, M.; Wu, X.; Garcia, S.J.; van der Zwaag, S. Direct and indirect observation of multiple local healing events in successively loaded fibre reinforced polymer model composites using healing agent-filled compartmented fibres. *Composites Science and Technology* **2015**, *106*, 127-133.
20. Norris, C.J.; Meadway, G.J.; O'Sullivan, M.J.; Bond, I.P.; Trask, R.S. Self-healing fibre reinforced composites via a bioinspired vasculature. *Advanced Functional Materials* **2011**, *21*, 3624-3633.
21. Tabaković, A.; Post, W.; Cantero, D.; Copuroglu, O.; Garcia, S.J.; Schlangen, E. The reinforcement and healing of asphalt mastic mixtures by rejuvenator encapsulation in alginate compartmented fibres. *Smart Materials and Structures* **2016**, *25*.
22. Van Stappen, J.; Bultreys, T.; Gilabert, F.A.; Hillewaere, X.K.D.; Gómez, D.G.; Van Tittelboom, K.; Dhaene, J.; De Belie, N.; Van Paepegem, W.; Du Prez, F.E.*, et al.* The microstructure of capsule containing self-healing materials: A micro-computed tomography study. *Materials Characterization* **2016**, *119*, 99-109.

23. Bekas, D.G.; Baltzis, D.; Tsirka, K.; Exarchos, D.; Matikas, T.; Meristoudi, A.; Pispas, S.; Paipetis, A.S. Self-healing polymers: Evaluation of self-healing process via non-destructive techniques. *Plastics, Rubber and Composites* **2016**, *45*, 147-156.
24. Pang, J.W.C.; Bond, I.P. A hollow fibre reinforced polymer composite encompassing self-healing and enhanced damage visibility. *Composites Science and Technology* **2005**, *65*, 1791-1799.
25. Kersemans, M.; De Baere, I.; Degrieck, J.; Van Den Abeele, K.; Pyl, L.; Zastavnik, F.; Sol, H.; Van Paepegem, W. Nondestructive damage assessment in fiber reinforced composites with the pulsed ultrasonic polar scan. *Polymer Testing* **2014**, *34*, 85-96.
26. Kersemans, M.; De Baere, I.; Degrieck, J.; Van Den Abeele, K.; Pyl, L.; Zastavnik, F.; Sol, H.; Van Paepegem, W. Damage signature of fatigued fabric reinforced plastics in the pulsed ultrasonic polar scan. *Experimental Mechanics* **2014**, *54*, 1467-1477.
27. Solodov, I.; Pfleiderer, K.; Gerhard, H.; Predak, S.; Busse, G. New opportunities for nde with air-coupled ultrasound. *NDT and E International* **2006**, *39*, 176-183.
28. Solodov, I.Y.; Stoessel, R.; Busse, G. Material characterization and nde using focused slanted transmission mode of air-coupled ultrasound. *Research in Nondestructive Evaluation* **2004**, *15*, 65-85.
29. Neuenschwander, J.; Furrer, R.; Roemmeler, A. Application of air-coupled ultrasonics for the characterization of polymer and polymer-matrix composite samples. *Polymer Testing* **2016**, *56*, 379-386.
30. Solodov, I. Resonant acoustic nonlinearity of defects for highly-efficient nonlinear nde. *Journal of Nondestructive Evaluation* **2014**, *33*, 252-262.
31. Solodov, I.; Bai, J.; Bekgulyan, S.; Busse, G. A local defect resonance to enhance acoustic wave-defect interaction in ultrasonic nondestructive evaluation. *Applied Physics Letters* **2011**, *99*.
32. Bose, R.K.; Hohlbein, N.; Garcia, S.J.; Schmidt, A.M.; van der Zwaag, S. Connecting supramolecular bond lifetime and network mobility for scratch healing in poly(butyl acrylate) ionomers containing sodium, zinc and cobalt. *Physical Chemistry Chemical Physics* **2015**, *17*, 1697-1704.
33. Varley, R.J.; van der Zwaag, S. Towards an understanding of thermally activated self-healing of an ionomer system during ballistic penetration. *Acta Materialia* **2008**, *56*, 5737-5750.
34. Hohlbein, N.; Shaaban, A.; Schmidt, A.M. Remote-controlled activation of self-healing behavior in magneto-responsive ionomeric composites. *Polymer (United Kingdom)* **2015**, *69*, 301-309.
35. Dong, J.; Ding, J.; Weng, J.; Dai, L. Graphene enhances the shape memory of poly (acrylamide-co-acrylic acid) grafted on graphene. *Macromolecular Rapid Communications* **2013**, *34*, 659-664.
36. Zhang, Z.; Hu, Y.; Liu, Z.; Guo, T. Synthesis and evaluation of a moisture-promoted healing copolymer. *Polymer* **2012**, *53*, 2979-2990.
37. Rodriguez, E.D.; Luo, X.; Mather, P.T. Linear/network poly(ε-caprolactone) blends exhibiting shape memory assisted self-healing (smash). *ACS Applied Materials and Interfaces* **2011**, *3*, 152-161.
38. Kumar, R.L.V.; Jawali, N.D.; Srikanth, L.; Kumar, C.R.; Prakash, M.R.; Rao, R.M.V.G.K. Post impact compression strength (pics) evaluation of glass/epoxy composite using a novel approach — effect of delamination area. *Journal of Reinforced Plastics and Composites* **2007**, *26*, 1101-1109.
39. Tan, K.T.; Watanabe, N.; Iwahori, Y.; Ishikawa, T. Effect of stitch density and stitch thread thickness on compression after impact strength and response of stitched composites. *Composites Science and Technology* **2012**, *72*, 587-598.
40. Wu, K.-W.; Lee, C.-L.; Chang, Y.-C.; Ong, C.-L. Compressive strength of delaminated and repaired composite plates. *Materials Chemistry and Physics* **1996**, *43*, 173-177.
41. Zhou, G. Effect of impact damage on residual compressive strength of glass-fibre reinforced polyester (gfrp) laminates. *Composite Structures* **1996**, *35*, 171-181.